Annihilation of structural defects in chalcogenide absorber films for high-efficiency solar cells

R. Mainz[a,*], E. Simsek Sanli[b], H. Stange[c], D. Azulay[d], S. Brunken[a], D. Greiner[a], S. Hajaj[d], M. D. Heinemann[a], C. A. Kaufmann[a], M. Klaus[a], Q. M. Ramasse[e], H. Rodriguez-Alvarez[a], A. Weber[a], I. Balberg[d], O. Millo[d], P. A. van Aken[b], D. Abou-Ras[a]

[a]*Helmholtz-Zentrum Berlin für Materialien und Energie GmbH, Hahn-Meitner-Platz 1, 14109 Berlin, Germany*
[b]*Max Planck Institute for Solid State Research, Stuttgart Center for Electron Microscopy, Heisenbergstr. 1, 70569 Stuttgart, Germany*
[c]*Technische Universität Berlin, Institut für Werkstoffwissenschaften, Ernst-Reuter-Platz 1, 10587 Berlin, Germany*
[d]*Racah Institute of Physics and the Center for Nanoscience and Nanotechnology, The Hebrew University of Jerusalem, Jerusalem 91904, Israel*
[e]*SuperSTEM Laboratory, SciTech Daresbury Campus, Keckwick Lane, Daresbury, WA4 4AD, United Kingdom*
* *Corresponding author: roland.mainz@helmholtz-berlin.de*

Electronic Supplementary Information

1 Supplementary Figures

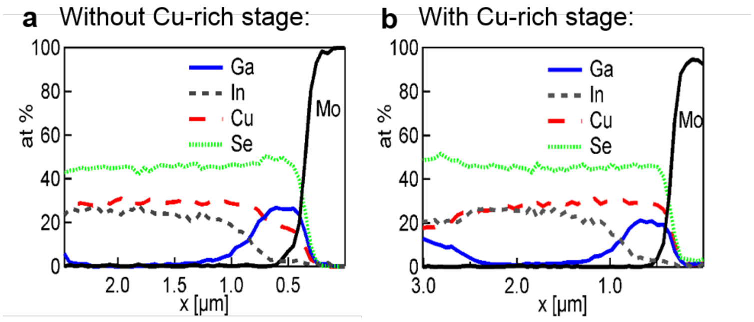

Figure S1 Compositional depth profiles recorded by SEM-EDX for the sample with (a) and without (b) Cu-rich stage.

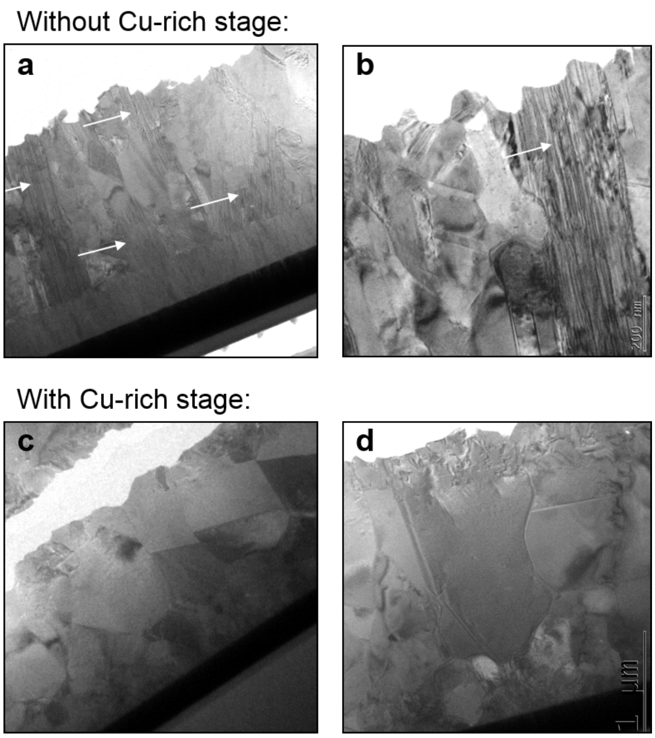

Figure S2 Bright-field TEM images for the sample that was synthesized without (a, b) and with (c, d) a Cu-rich process stage.

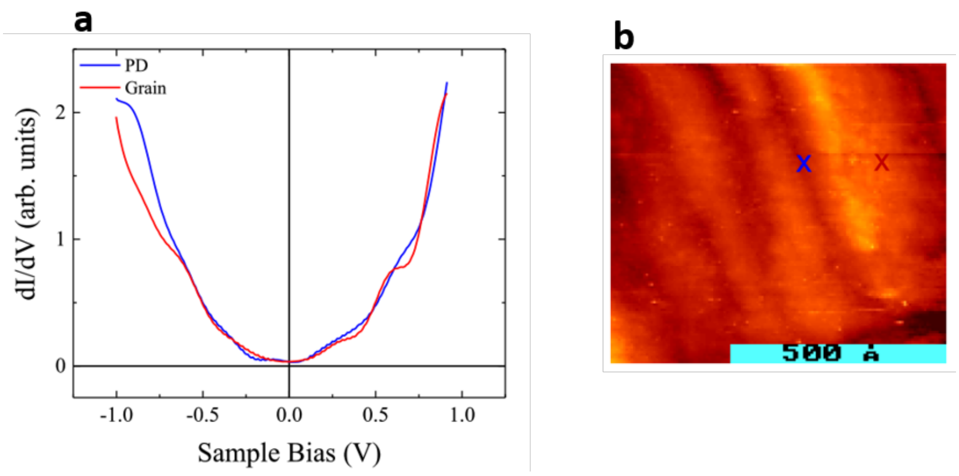

Figure S3 (a) STS measurement on a planar defect (PD) and on an adjacent grain for the sample processed without Cu-rich stage. The spots where the STS data were recorded are marked in the STM image in (b).

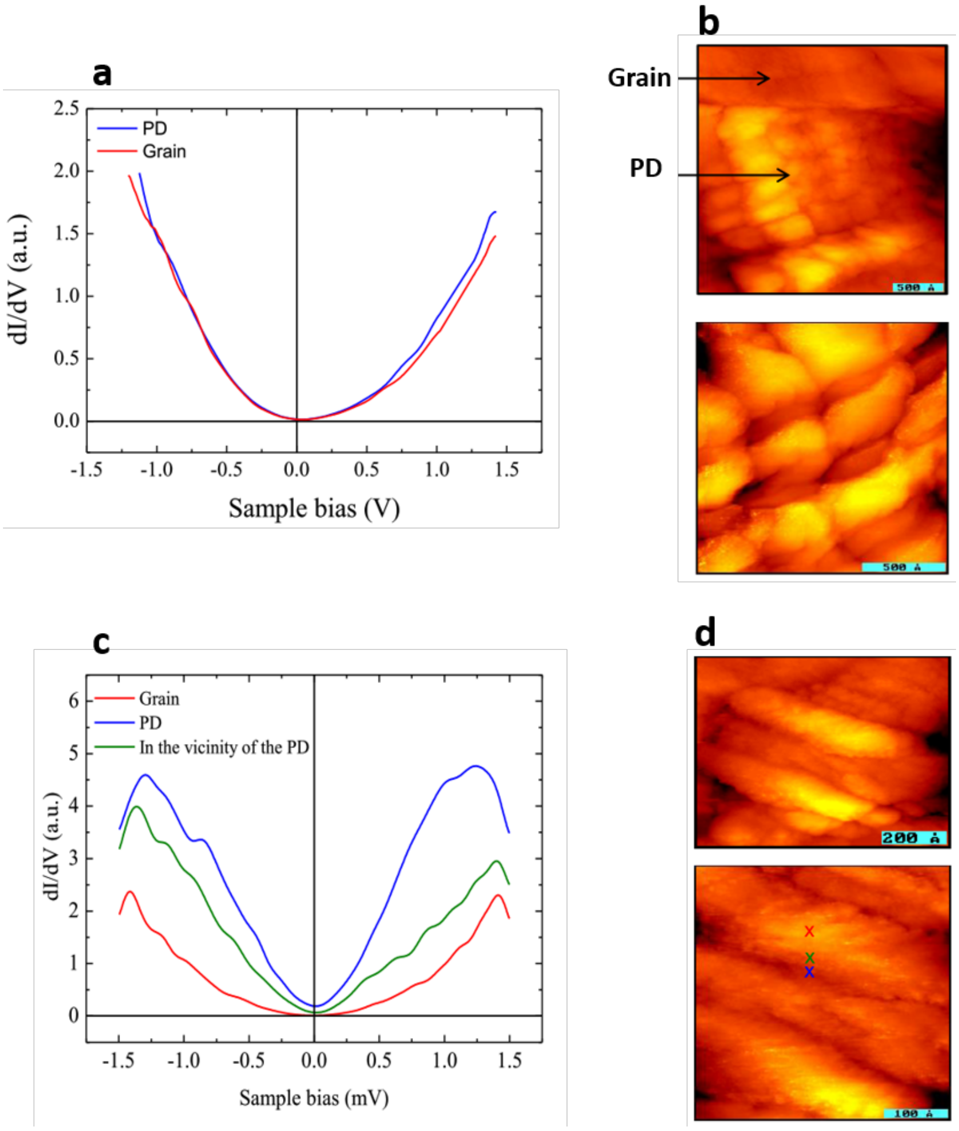

Figure S4 (a,c) STS measurement on a planar defect (PD) and on a grain for the sample processed with Cu-rich stage. The spots where the STS data in (a) and (c) were recorded are marked in the STM images in (b) and (d) respectively. In each pair of images in (b) and (d), the lower image zooms on an area within the upper one.

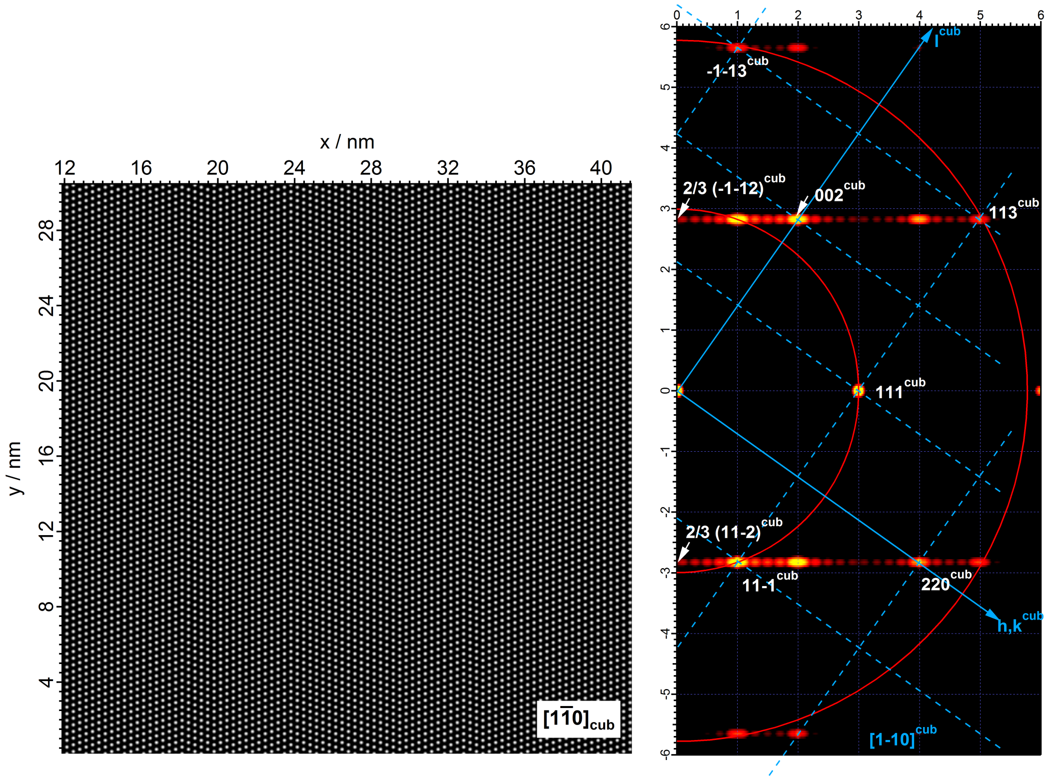

Figure S5 Left: Subsection of a model lattice image of a fcc lattice with twin faults in the $(111)_{\mathrm{cub}}$ planes. The twin faults were introduced randomly with a fault probability of 6%. A Fast Fourier transformation (FFT) of the complete image with a range of 100 nm on the x-axis resulted in the figure shown on the right.

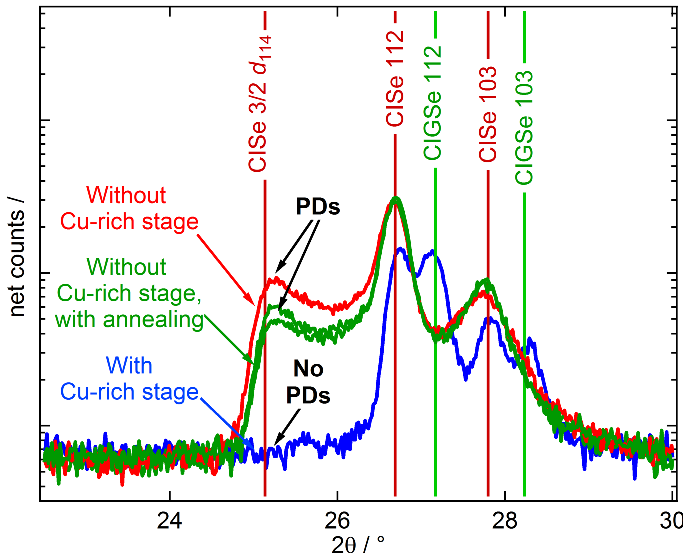

Figure S6 *Ex-situ* grazing incidence (GI) XRD measured on the sample processed *without a Cu-rich stage*, *without a Cu-rich stage but with additional annealing*, and *with a Cu-rich process stage*. The thermal history of the sample grown *without Cu-rich stage but with annealing* (i.e. time of exposure to maximum substrate temperature of 430 ℃) was equal to that of the sample grown with Cu-rich stage. See Methods of the main paper for details. The two green lines (labeled *Without Cu-rich stage, with annealing*) were measured on two different positions.

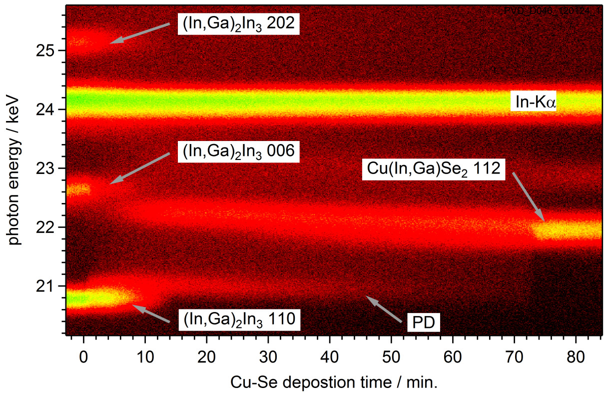

Figure S7 Color-coded EDXRD spectra as function of energy and Cu-Se deposition time, showing the transition from $(In,Ga)_2Se_3$ to the tetragonal Cu-In-Ga-Se phase with planar defects (PD) at a substrate temperature of 450 ℃.

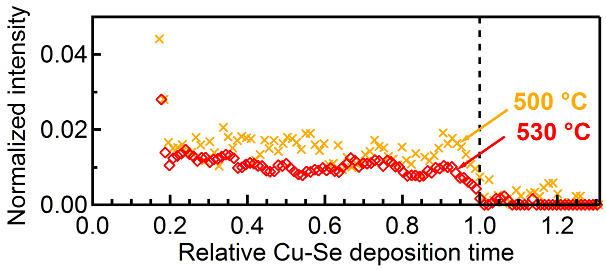

Figure S8 Normalized PD signal intensities during Cu-Se deposition onto $(In,Ga)_2Se_3$ films at 500 ℃ and 530 ℃ substrate temperature. The vertical dashed line marks the Cu-poor to Cu-rich transition. The data for 530 ℃ equals that shown in Fig. 5d in the main text.

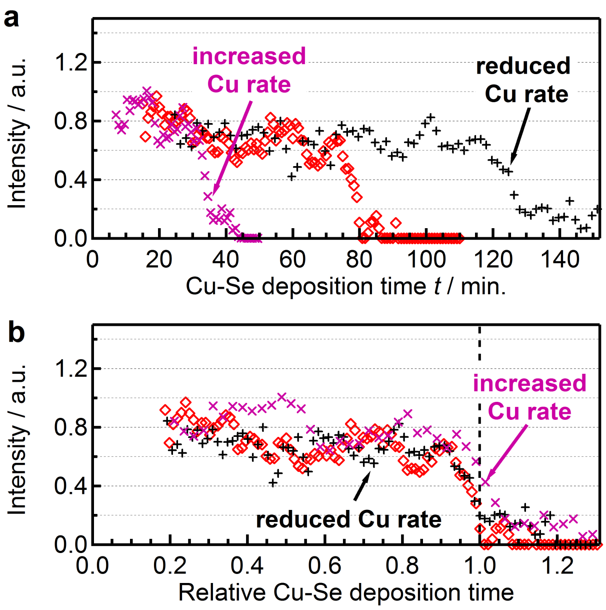

Figure S9 PD signal intensities during Cu-Se deposition onto $(In,Ga)_2Se_3$ films at 530 ℃ substrate temperature with reduced (black), normal (red), and increased (violet) Cu deposition rate plotted (a) vs. Cu-Se deposition time and (b) vs. relative Cu-Se deposition time. The vertical dashed line in (b) marks the Cu-poor to Cu-rich transition. The relative Cu-Se deposition time of 1 corresponds to 128 min. for the reduced Cu rate, 80 min. for the normal rate, and 33 min. for the increased rate. This means that the reduced Cu deposition rate was 0.63 times that of the normal rate, and the increased rate was 2.4 times that of the normal rate. The data with normal deposition rate (red) equals that shown in Fig. 5d in the main text.

2 Supplementary Methods

SEM-EDX: Elemental depth profiles were measured on fracture cross-sections by energy dispersive X-ray spectroscopy (EDX) in a Leo1530 scanning electron microscope (SEM).

Additional information on C-AFM: Since the scan rate was such that the tip stayed locally within the given contact area for less than 1 ms, the electron dose was rather low, of only 1018 electrons/cm2. Consequently, the sample was not damaged in the course of measurements, as manifested by the reproducibility of our topography and current maps. An original feature in our C-AFM measurements is the ability to acquire simultaneously both dark current and photocurrent images (along with the topography) under identical tip pressure (and electrical contact). This is achieved by implementing a two-pass technique, in which the current in the second pass is measured with the AFM laser turned off (using the stored topographic information gained during the first pass). In this way, the dark and photocurrent measurements are performed on exactly the same location, with identical tip pressure (or electrical contact). This method thus allows separating dark from photo effects also for materials with a bandgap smaller than the photon energy of the AFM laser. The AFM laser intensity (1 mW) is focused to a 100 mm diameter. The light impinges on the tip-sample contact area after scattering by the cantilever as the cantilever shades the tip-sample contact area. As a result only a few percent of the original intensity reaches the relevant area. Considering these two factors leads to an estimated illumination intensity of the order of one to a few suns, comparable to that in operating solar cells. In addition, since the space-charge region width is typically of the order of a few Debye (20-40 nm) lengths ($\sim$100 nm), also the electric field at the tip/sample interface is similar to that operative in a working solar cell, $\sim$ 104 V/cm.